Supplemental Material

Bispecific antibody-mediated redirection of NKG2D-CAR natural killer cells facilitates dual targeting and enhances antitumor activity

Congcong Zhang, Jasmin Röder, Anne Scherer, Malena Bodden,

Jordi Pfeifer Serrahima, Anita Bhatti, Anja Waldmann, Nina Müller,

Pranav Oberoi, Winfried S. Wels

This document includes:

Zhang C, *et al. J Immunother Cancer* 2021; 9:e002980. doi: 10.1136/jitc-2021-002980

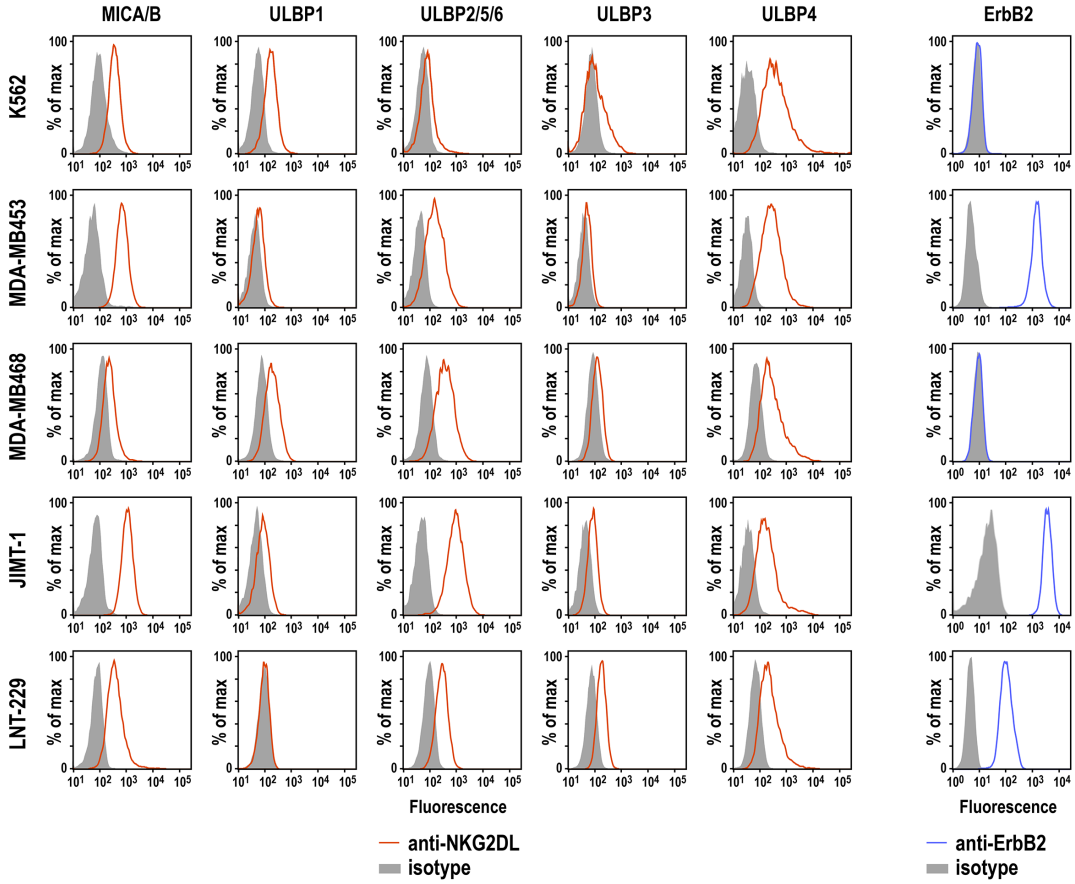

Supplementary Figure S1 Surface expression of NKG2D ligands (NKG2DL) by K562 erythroleukemia cells, MDA-MB453, MDA-MB468 and JIMT-1 breast carcinoma cells, and LNT-229 glioblastoma cells was determined by flow cytometry with BV786-conjugated anti-human MICA/B antibody (BD Biosciences), APC-conjugated anti-ULBP1 antibody, APC-conjugated anti-ULBP2/5/6 antibody, PE-conjugated anti-ULBP3 antibody, and PE-conjugated anti-ULBP4 antibody (all R&D Systems) (left panels; solid red lines). Cells treated with isotype antibodies served as controls (left panels; filled areas). Surface expression of ErbB2 by the same cancer cell lines was determined using APC-conjugated anti-ErbB2 antibody 24D2 (BioLegend) (right panels; solid blue lines). Cells stained with an isotype antibody were included as controls (right panels; filled areas).

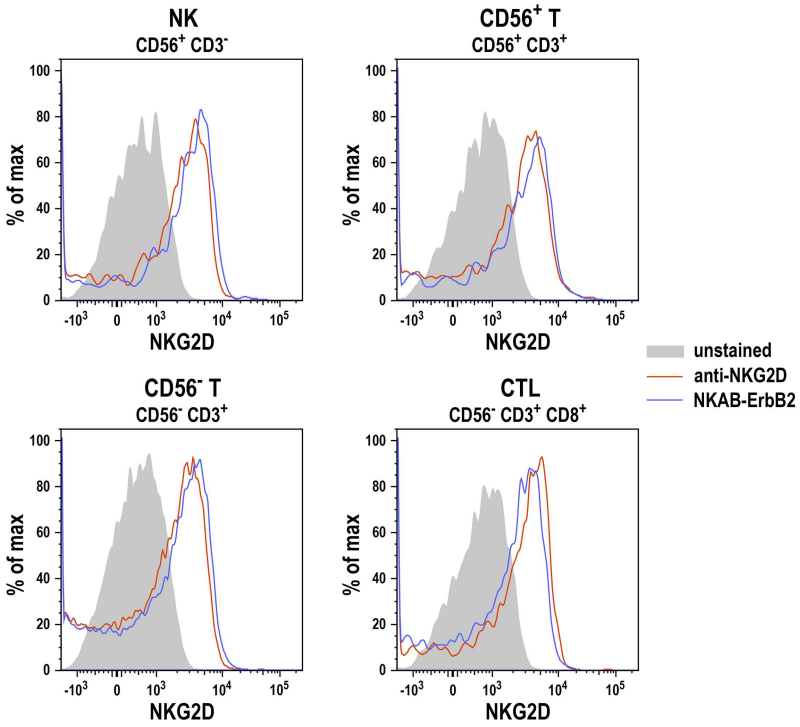

Supplementary Figure S2 Binding of NKAB-ErbB2 to NKG2D-positive lymphocytes. Freshly isolated PBMCs were incubated with Fc Block and then stained with PerCP-conjugated anti-CD45, BV421-conjugated anti-CD56, V500-conjugated anti-CD3, and PE-Cy7-conjugated anti-CD8 antibodies. For detection of NKG2D, cells were in addition stained with APC-conjugated anti-NKG2D antibody or APC-conjugated purified NKAB-ErbB2 protein. Shown are NK cells ($CD56^+$ $CD3^-$), CD56-postitive T cells ($CD56^+$ $CD3^+$), CD56-negative T cells ($CD56^-$ $CD3^+$) and cytotoxic T cells ($CD56^-$ $CD3^+$ $CD8^+$) detected with anti-NKG2D or NKAB-ErbB2 in comparison to unstained control cells among CD45-positive cells gated according to their surface marker expression. Data for a representative donor are shown.

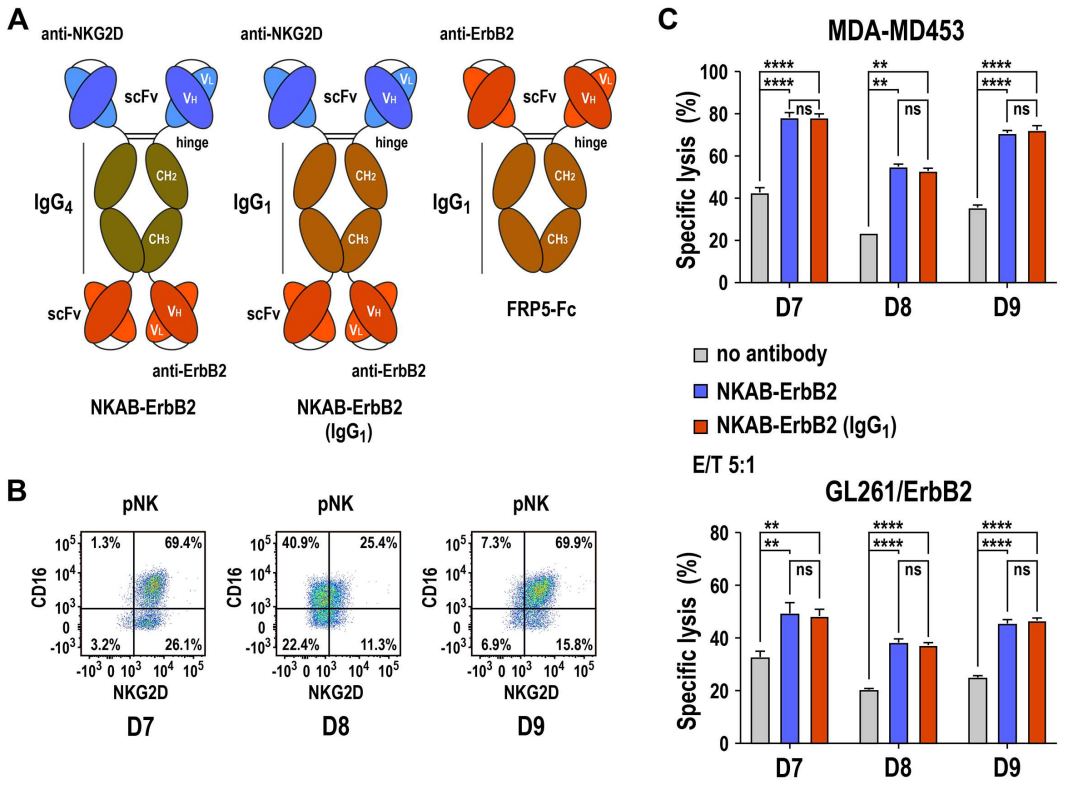

Supplementary Figure S3 (A) Schematic representation of bispecific antibody NKAB-ErbB2 with hinge, CH_2 and CH_3 domains of human IgG_4 (left), the similar NKAB-ErbB2 (IgG_1) molecule carrying a human IgG_1 Fc region instead of IgG_4 (middle), and the ErbB2-specific mini-antibody FRP5-Fc harboring an N-terminal scFv fragment derived from ErbB2-specific antibody FRP5, hinge, CH_2 and CH_3 domains of human IgG_1 (right) used in the experiments shown in Figure 4. Disulfide bridges connecting the monomers within the homodimeric molecules are indicated by lines. (B) Expression of NKG2D and CD16 by *ex vivo* expanded peripheral blood NK cells (pNK) from healthy donors (D7-D9) was analyzed by flow cytometry with anti-NKG2D and anti-CD16 antibodies as indicated. (C) Cytotoxicity of the pNK cells shown in (B) against ErbB2-expressing MDA-MB453 breast carcinoma cells (upper) and murine GL261/ErbB2 cells expressing human ErbB2 but no ligands cross-reactive with human NKG2D (lower) in the absence of bispecific antibody (gray bars), or in the presence of 0.64 nM (100 ng/mL) IgG_4-based NKAB-ErbB2 (blue bars) or the similar IgG_1-based NKAB-ErbB2 (IgG_1) molecule (red bars) was investigated in FACS-based cytotoxicity assays after co-incubation at an effector to target ratio (E/T) of 5:1 for 3 hours. Mean values ± SD are shown; n=3 technical replicates for each donor. Data were analyzed by two-tailed unpaired Student's *t*-test. ****, $p < 0.0001$; **, $p < 0.01$; ns: not significant ($p > 0.05$).

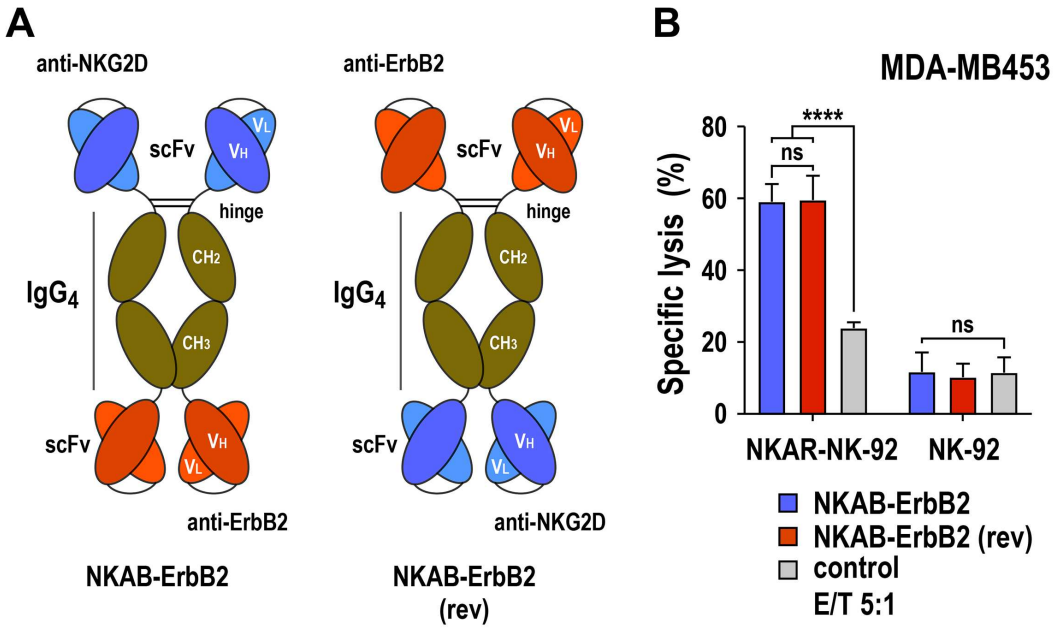

Supplementary Figure S4 Comparative analysis of bispecific antibodies NKAB-ErbB2 and NKAB-ErbB2 (rev). (A) Schematic representation of NKAB-ErbB2 harboring an NKG2D-specific scFv fragment at the N-terminus, followed by hinge, CH_2 and CH_3 domains of human IgG_4, a $(G_4S)_2$ linker, and a C-terminal ErbB2-specific scFv fragment (left), and NKAB-ErbB2 (rev), in which the positions of NKG2D- and ErbB2-specific antibody domains are switched (right). (B) The effects of NKAB-ErbB2 (blue bars) and NKAB-ErbB2 (rev) (red bars) on specific cytotoxicity of NKAR-NK-92 (left) and parental NK-92 cells (right) against ErbB2-positive MDA-MB453 breast carcinoma cells was determined in FACS-based cytotoxicity assays after co-incubation at an effector to target ratio (E/T) of 5:1 for 3 hours in the absence (gray bars) or presence of 0.32 nM (50 ng/mL) of bispecific antibodies. Mean values ± SD are shown; n=4 technical replicates. Data were analyzed by two-tailed unpaired Student's *t*-test. ****, $p < 0.0001$; ns: not significant ($p > 0.05$).

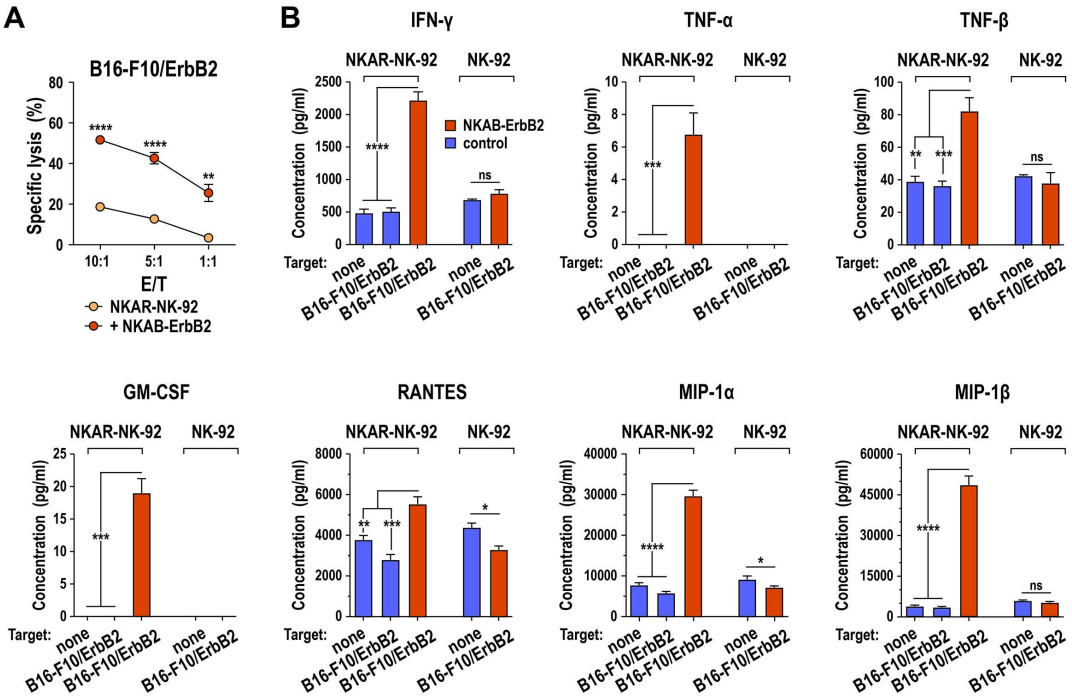

Supplementary Figure S5 Activity of NKAB-ErbB2 and NKAR-NK-92 against ErbB2-expressing melanoma cells. (A) Cytotoxicity of NKAR-NK-92 in the absence (orange circles) or presence (red circles) of 0.16 nM (25 ng/mL) of NKAB-ErbB2 against murine B16-F10/ErbB2 melanoma cells expressing human ErbB2 was investigated in FACS-based cytotoxicity assays after co-incubation at different E/T ratios for 3 hours. Mean values ± SD are shown; n=3 technical replicates from a representative experiment. (B) NKAR-NK-92 or parental NK-92 cells at a density of 5 x 10^5 cells/mL were incubated for 6 hours with B16-F10/ErbB2 cells at an E/T ratio of 1:1 in the absence (blue bars) or presence (red bars) of 0.16 nM (25 ng/mL) NKAB-ErbB2 as indicated. NK cells kept in the absence of tumor cells were included as controls. Supernatants were collected and the levels of IFN-γ, TNF-α, TNF-β, GM-CSF, RANTES (CCL5), MIP-1α (CCL3) and MIP-1β (CCL4) were measured using a cytometric bead array. Mean values ± SD are shown; n=3 technical replicates. Data in (A) and (B) were analyzed by two-tailed unpaired Student's *t*-test. ****, $p < 0.0001$; ***, $p < 0.001$; **, $p < 0.01$; *, $p < 0.05$; ns: not significant ($p > 0.05$).

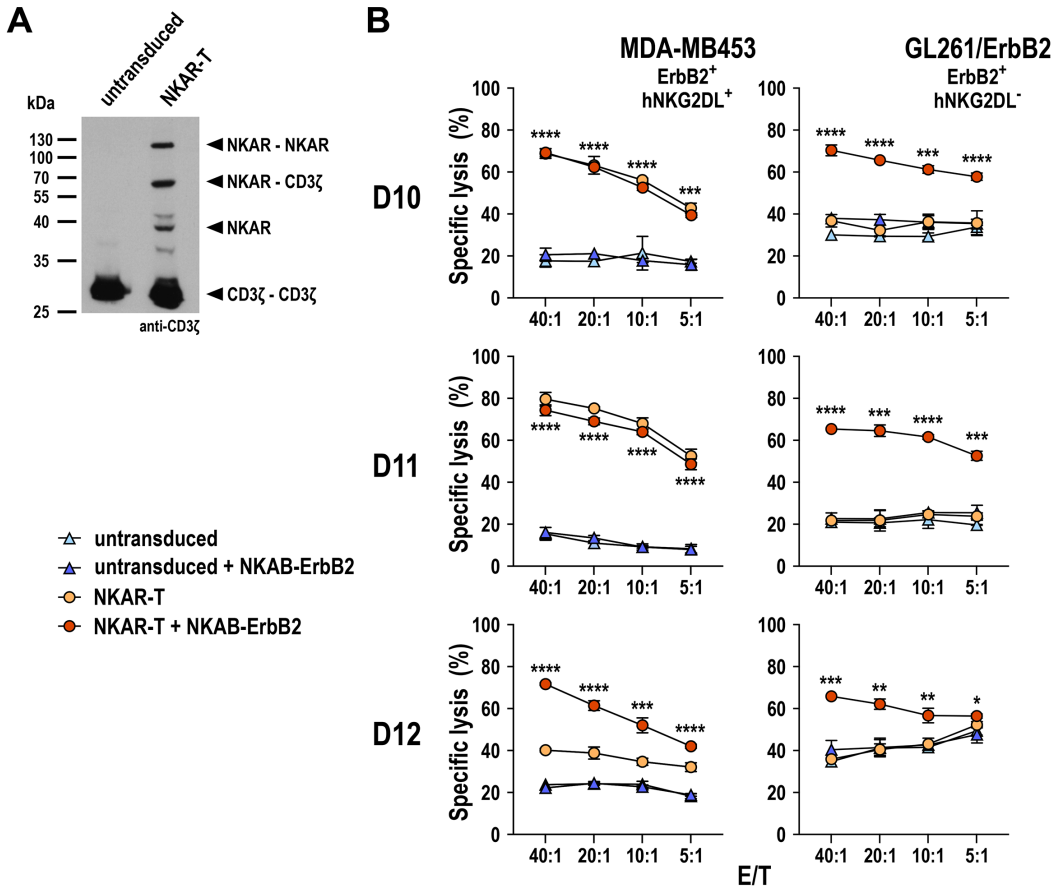

Supplementary Figure S6 Generation and functional characterization of NKAR-T cells. Peripheral blood mononuclear cells (PBMC) from healthy donors were stimulated overnight with immobilized anti-CD3 and anti-CD28 antibodies. Activated PBMCs were then cultured for three days in medium containing IL-2, before transduction with VSV-G pseudotyped NKAR-encoding lentiviral particles. Five to six days later, successfully transduced cells were enriched by flow cytometric cell sorting according to their EGFP expression. (A) Expression of NKAR by transduced T cells was analyzed by SDS-PAGE of whole cell lysate under non-reducing conditions and immunoblotting with CD3ζ-specific antibody, followed by HRP-conjugated secondary antibody and chemiluminescent detection. Lysate of untransduced T cells was included as control. The positions of NKAR homodimers and monomers, CD3ζ homodimers, and NKAR-CD3ζ heterodimers are indicated by arrowheads. Data from a representative donor are shown. (B) Cytotoxicity of NKAR-T (orange circles) and untransduced T cells (light blue triangles) in the absence, and NKAR-T (red circles) and untransduced T cells (dark blue triangles) in the presence of 0.64 nM (100 ng/mL) of bispecific NKAB-ErbB2 antibody against human MDA-MB453 breast carcinoma cells endogenously expressing ErbB2 and NKG2D ligands (left) and murine GL261/ErbB2 glioblastoma cells stably expressing human ErbB2 but no NKG2D ligands reactive with human NKG2D (right) was investigated in FACS-based cytotoxicity assays after co-incubation at different E/T ratios for 3 hours. Mean values ± SD are shown; n=3 technical replicates for each donor. Data were analyzed by two-tailed unpaired Student's *t*-test (shown for NKART-T cells + NKAB-ErbB2 versus untransduced T cells + NKAB-ErbB2). ****, $p < 0.0001$; ***, $p < 0.001$; **, $p < 0.01$; *, $p < 0.05$.

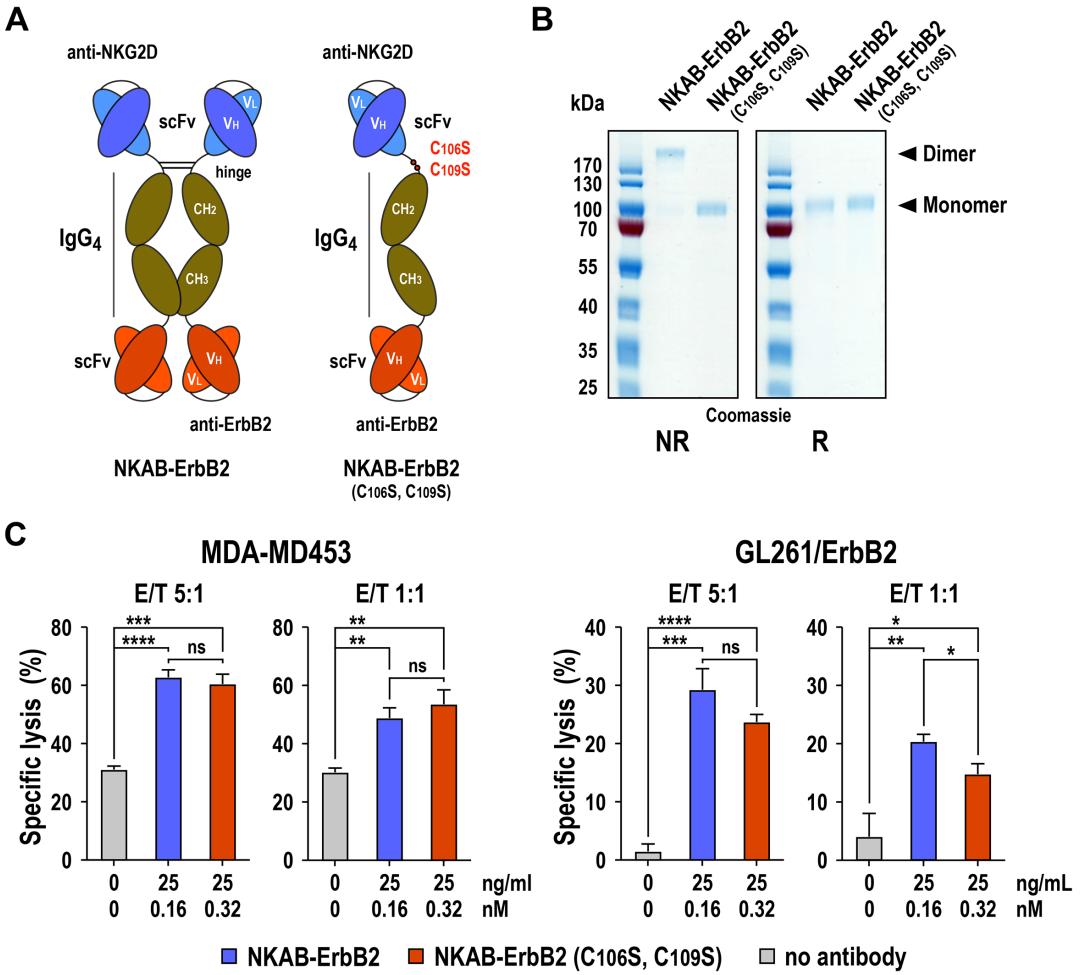

Supplementary Figure S7 (A) Schematic representation of bispecific antibody NKAB-ErbB2 with intact intermolecular disulfide bridges within the IgG_4 hinge region (left) and mutated monomeric NKAB-ErbB2 ($C_{106}S$, $C_{109}S$) wherein the cysteine residues within the hinge region are replaced by serine residues. (B) Analysis of purified NKAB-ErbB2 and NKAB-ErbB2 ($C_{106}S$, $C_{109}S$) proteins by SDS-PAGE under non-reducing (NR) or reducing conditions (R) and Coomassie staining. The positions of NKAB-ErbB2 monomers and homodimers are indicated. NKAB-ErbB2 ($C_{106}S$, $C_{109}S$) protein was expressed in HEK 293T cells and purified as described in Materials & Methods for NKAB-ErbB2. (C) Specific cytotoxicity of NKAR-NK-92 cells against ErbB2-positive human MDA-MB453 breast carcinoma cells (left) or murine GL261/ErbB2 cells expressing human ErbB2 but no ligands cross-reactive with human NKG2D (right) in the absence of bispecific antibody (gray bars) or in the presence of dimeric NKAB-ErbB2 (blue bars) or monomeric NKAB-ErbB2 ($C_{106}S$, $C_{109}S$) (red bars) was determined in FACS-based cytotoxicity assays after co-incubation at an effector to target ratio (E/T) of 5:1 or 1:1 for 3 hours. To correct for the different number of binding sites in homodimers and monomers, equal ng/mL concentrations of the proteins were used. Mean values ± SD are shown; n=3 technical replicates. Data were analyzed by two-tailed unpaired Student's *t*-test. ****, $p < 0.0001$; ***, $p < 0.001$; **, $p < 0.01$; *, $p < 0.05$; ns: not significant ($p > 0.05$).

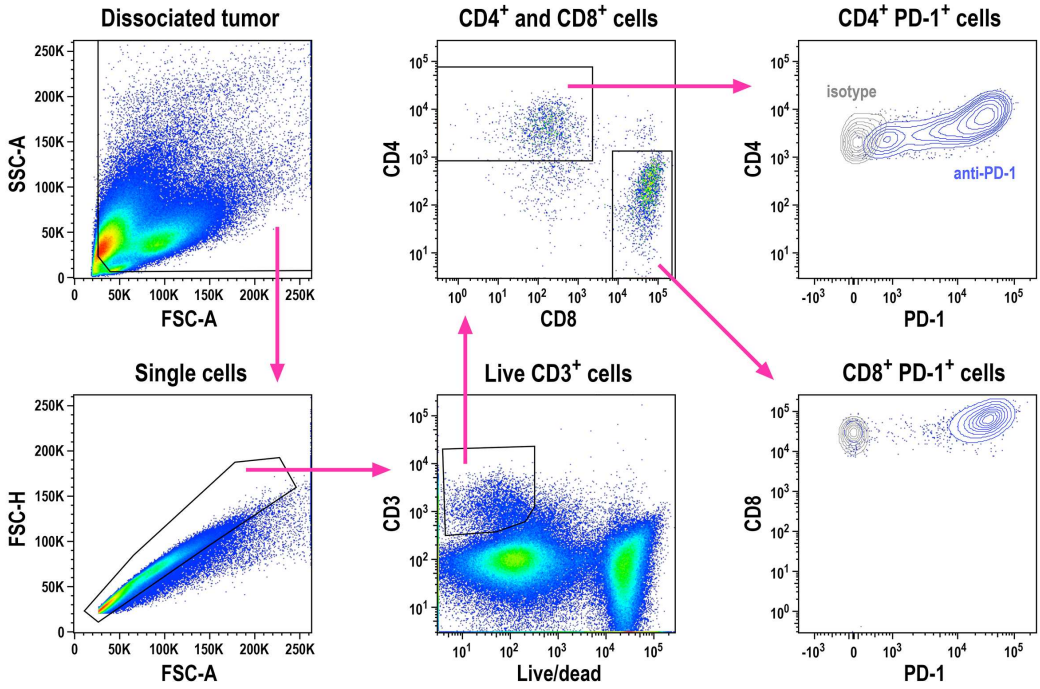

Supplementary Figure S8 Gating strategy applied for the analysis of tumor-infiltrating lymphocytes. PD-1 expression by $CD4^+$ and $CD8^+$ T cells within the population of live $CD3^+$ cells of singularized cells from dissociated tumor tissues was assessed with a PD-1-specific antibody as indicated. An irrelevant antibody of the same isotype served as a control. Exemplary data from one of the animals shown in Figure 7E treated with the combination of NKAR-NK-92 cells and NKAB-ErbB2 are shown. PD-1 expression by $CD4^+$ and $CD8^+$ T cells from spleen and peripheral blood was determined in the same manner.